INFLUENCE OF UPSTREAM FLOW CHARACTERISTICS ON THE REATTACHMENT PHENOMENON IN SHALLOW CAVITIES

by

Fatima MADI AROUS* *, *Amina MATAOUI, and Zahia BOUAHMED

LMFTA, Faculty of Physics, University of Science and Technology Houari Boumediene,
Bab Ezzouar, Algiers, Algeria

Original scientific paper
UDC: 532.528
DOI: 10.2298/TSCI101203019M

The influence of the upstream flow characteristics on the behaviour of the flow over a shallow cavity and on the reattachment phenomenon is examined. Accordingly, a comparison of the cavity's flow structure is performed for two different upstream flows: the wall jet flow and the boundary layer flow. The wall jet possesses a particular structure with two regions: an inner layer analogous to that of a boundary layer and an outer layer similar to that of a free jet; this layer is an additional source of turbulence production in addition to that of the inner shear layer. The present study interested to the effect of this external layer on the shallow cavity's flow. The numerical approach is based on the low Reynolds stress omega turbulence model. Fluent 6.3 and the pre-processor Gambit 2.3 are used for the computation. The numerical results indicate that the flow structure is very sensitive to the upstream flow's characteristics. Indeed, for the same Reynolds number and the same boundary layer thickness at the cavity leading edge, the cavity flow structure in a wall jet upstream flow case differs considerably from that of a boundary layer upstream flow. The most important finding is the earlier reattachment process in the wall jet inflow case, where an important reduction of the reattachment length is observed compared to that of a cavity under a boundary layer flow.

Key words: *cavity flow, wall jet, boundary layer, turbulence models, reattachment*

Introduction

Despite the simplicity of the geometric shape, the cavity flows engender the phenomena of separation and reattachment and are characterized by the presence of recirculation currents. Separated and reattaching flows play an important role in various engineering applications; they have been the subject of many investigations but remain still far from being fully mastered. Numerous researches were motivated by the need to understand these phenomena which are not related only to this configuration but also to the flows over steps and around obstacles. To control flow separation, many investigations have been conducted in fluids engineering. By the introduction of a periodical oscillating jet at the

* Corresponding author; e-mail: fmadi@usthb.dz; madi.fatima@yahoo.fr

step edge, Mehrez *et al.* [1] have examined the control of flow and mass transfer in separated and reattaching flow over a backward facing step. Mushatet [2] has studied the backward facing step turbulent flow with presence of ribs turbulators. The purpose of this study is to explore the effect of the ribs on feature of the flow, particularly on the strength and on the size of the recirculation zones, and on the heat transfer of the backward facing step in confined flows. Logan *et al.* [3] investigate the effect of the flows produced by buildings or natural obstacles in the vicinity of airports. Indeed, shear layers or wakes produced downwind of surface obstacles can prove hazardous to aircraft. Numerous researches were focused on this problem by the determination of the locations of these regions and their effects on aeronautical systems. Oka *et al.* [4] studied a flow field past a two dimensional square rod. They measured the velocity and turbulence in the recirculation zone located behind a rod placed in a rectangular channel wall. Oka [5] has conducted a series of experiments with the aim to determine the size and the shape of the vortices formed between two roughness elements and those in the free shear layer located at the roughness height. The results of this study show that the flow structure between two square roughness is similar to that of a shallow cavity. The cavity under a boundary layer flow was the subject of a great number of researches for more than fifty years. However, there are few studies concerning cavities under a wall jet flow which are focused mainly on the noise produced by this configuration. Steps and cavities under a wall jet flow are omnipresent in several environmental problems. Indeed, during thunderstorms, the wind spreads on the ground in a similar manner to that of wall jet flow [6]. Likewise, the wall jets have multiple applications such as environmental discharges, heat exchangers, fluid injection systems and cooling of combustion chamber wall in a gas turbine [7]. The wall jet is characterised by the presence of two zones: the inner layer extending from the wall to the maximum velocity location, similar to the boundary layer type, and the outer layer that extends from the maximum velocity location at the outer border which is similar to the free jet [8, 9]. This particular characteristic of a wall jet prompted us to study the jet-cavity interaction and to compare the flow structure to that of a cavity under a boundary layer flow, in order to analyse the turbulence effect of the external layer's turbulence of a turbulent wall jet on the evolution of the shallow cavity's flow structure. Recently, a number of studies of wall jet-backward facing step interaction have been conducted. Badri [10] studied experimentally, by hot wire measurements, the effect of the wall's roughness and the external turbulence rate on the flow structure over a backward facing step. His researches concluded that the effects of the external turbulence rate on the reattachment length and on the recirculation zone's structure are very significant. However, in the wall jet incoming flow, the reattachment length is shorter compared to that of the boundary layer. Similar findings are obtained by Jacob *et al.* [11] and by Nait Bouda *et al.* [12]. Ganesh *et al.* [13] was interested to the noise produced by the jet-cavity interaction. This study was motivated by the need to understand the cavity's flow evolution well enough to devise effective cavity resonance suppression technique. Two important findings emerge from this study. First, the jet cavity interaction produces a unique set of tones, different of cavity tones or jet tones. Second, based on earlier research, the traditional classifications (open, transitional, or closed) for cavities in a free flow stream would be insensitive to small variations of a Mach number and would depend primarily on the cavity's length/depth ratio. However, this study shows that these classifications are actually quite sensitive to the jet Mach number.

The cavity flow is a 3-D physical phenomenon, but a small length to width cavity's ratio L/W favours the establishment of a 2-D behaviour [14]. Ahuja *et al.* experiments [15] showed that the cavity flow is essentially 2-D for $L/W < 1$. Numerous studies have shown that the 2-D simulation constitutes a good approximation [16-18]. In view of that, we considered in the present study a 2-D turbulent cavity flow. The purpose of this study is examining the influence of the inflow characteristics on the flow behaviour of shallow cavities, particularly on the reattachment phenomenon. Accordingly, the comparison of cavities' flow structures was carried out for two different upstream flows: a boundary layer flow and a wall jet flow. The comparison was performed for three different cavities of large aspect ratio: $AR = 14$, $AR = 12$, and $AR = 10$.

Formulation of the problem

The geometrical parameters of the problems considered in this study, the Reynolds number and the boundary layer thickness at leading edge ($x = 0$) are identical to those of the experiments of Badri [10] and those of Nait Bouda *et al.* [12]. The cavities' depth H is equal to 2 cm, the nozzles' height b is equal to 4 cm, the distance between the jet exit and the cavity D is equal to 110 cm, the Reynolds number and the boundary layer thickness at the leading edge are equal to 7600 and 2 cm, respectively, for both incoming flows considered in this study.

The governing equations

The flow fields for 2-D, incompressible, isotherm and statistically steady flow are governed by the following conservative equations in Cartesian tensor notations:

– mass
$$\frac{\partial U_j}{\partial x_j} = 0 \tag{1}$$

– momentum
$$U_j \frac{\partial U_i}{\partial x_j} = -\frac{1}{\rho}\frac{\partial P}{\partial x_i} + \frac{\partial}{\partial x_j}\left[\nu \frac{\partial U_i}{\partial x_j} - \overline{u_i u_j}\right] \tag{2}$$

where ν is the kinematic viscosity and U_j – the velocity component in the j-direction.

Turbulence modelling

The closure of the governing equations is realised by the low-Re stress omega model. It is a stress-transport model based on the omega equation and Launder, Reece, and Rodi (LRR) model. The low-Re stress omega is a multi-scale model which has a wide range of applications. This model has proven to be accurate for wall-bounded flows, including separation [19]. The low-Re stress-omega solves the Reynolds' stresses transport equations in addition to an equation for the specific dissipation rate ω. This means that five additional transport equations are required in 2-D flows. Kolmogorov defined ω as the rate of energy dissipation per unit volume and time; the inverse of ω is the time scale along which dissipation of turbulence energy occurs [19].

The exact equation of the Reynolds stress τ_{ij}, for an incompressible and statistically steady flow, is in the following form [19]:

$$U_k \frac{\partial \tau_{ij}}{\partial x_k} = -P_{ij} + \frac{2}{3}\beta^* \omega k \delta_{ij} - \Pi_{ij} + \frac{\partial}{\partial x_k}\left[(\nu + \sigma^* \nu_t) \frac{\partial \tau_{ij}}{\partial x_k} \right] \tag{3}$$

The omega equation is written as follows:

$$U_j \frac{\partial \omega}{\partial x_j} = \alpha \frac{\omega}{k} \tau_{ij} \frac{\partial U_i}{\partial x_j} - \beta \omega^2 + \frac{\partial}{\partial x_k}\left[(\nu + \sigma \nu_t) \frac{\partial \omega}{\partial x_k} \right] \tag{4}$$

where $\sigma = \sigma^* = 1/2$ and the turbulent viscosity ν_t is given by $\nu_t = \alpha^*(k/\omega)$ (5)

where α^* is a function of the turbulent Reynolds number and is given by:

$$\alpha^* = \frac{\frac{36}{125} + R_{eT}}{12 + R_{eT}} \tag{6}$$

The turbulence Reynolds number R_{eT} is defined by:

$$R_{eT} = \frac{k}{\omega \nu} \tag{7}$$

β^* is a function of the turbulent Reynolds number defined by:

$$\beta^* = \frac{9}{100} \left(\frac{\frac{4}{15} + \frac{R_{eT}}{12}}{1 + \frac{R_{eT}}{12}} \right) f_{\beta^*} \tag{8}$$

f_{β^*} verifies the condition of eq. (9)

$$f_{\beta^*} = \begin{cases} 1 \quad if \quad \chi_k \le 0 \\ \dfrac{1 + 640\chi_k^2}{1 + 400\chi_k^2} \end{cases} \quad \text{if} \quad \chi_k > 0, \qquad \chi_k = \frac{1}{\omega^3} \frac{\partial k}{\partial x_j} \frac{\partial \omega}{\partial x_j} \tag{9}$$

α is also a function of the turbulent Reynolds number given by:

$$\alpha = \alpha_\infty \left(\frac{\alpha_0 R_\omega + R_{eT}}{R_\omega + R_{eT}} \right) \left(\frac{3R_\omega + R_{eT}}{3\alpha_0^* R_\omega + R_{eT}} \right) \tag{10}$$

where α_∞, α_0, and R_ω are model constants equal to 0.52, 0.21, and 6.20, respectively, (11)

and

$$\beta = \frac{9}{125} f_\beta \tag{12}$$

where

$$f_\beta = \frac{1 + 70\chi_\omega}{1 + 80\chi_\omega}, \qquad \chi_\omega = \left| \frac{\Omega_{ij} \Omega_{jk} S_{ki}}{(0.09\omega)^3} \right| \tag{13}$$

Ω_{ij} and S_{ki} are, respectively, the mean-strain-rate and the mean-rotation tensors defined as:

$$S_{ij} = \frac{1}{2}\left(\frac{\partial U_i}{\partial x_j} + \frac{\partial U_j}{\partial x_i}\right), \quad \Omega_{ij} = \frac{1}{2}\left(\frac{\partial U_i}{\partial x_j} - \frac{\partial U_j}{\partial x_i}\right) \tag{14}$$

The stress omega model does not require a wall-reflexion term in pressure-strain term Π_{ij} which can be written for the low-Re stress omega model as:

$$\Pi_{ij} = \beta^* C_1 \omega\left(\tau_{ij} + \frac{2}{3}k\delta_{ij}\right) - \hat{\alpha}\left(P_{ij} - \frac{2}{3}P\delta_{ij}\right) - \hat{\beta}\left(D_{ij} - \frac{2}{3}P\delta_{ij}\right) - \hat{\gamma}k\left(S_{ij} - \frac{1}{3}S_{kk}\delta_{ij}\right) \tag{15}$$

where
$$P_{ij} = \tau_{im}\frac{\partial U_j}{\partial x_m} + \tau_{jm}\frac{\partial U_i}{\partial x_m}, \quad D_{ij} = \tau_{im}\frac{\partial U_m}{\partial x_j} + \tau_{jm}\frac{\partial U_m}{\partial x_i}, \quad P = \frac{1}{2}P_{kk} \tag{16}$$

The closure coefficients, when low Re number correction is included, are given by:

$$\hat{\alpha} = \frac{12 + \hat{\alpha}_\infty R_{\mathrm{eT}}}{12 + R_{\mathrm{eT}}}, \quad \hat{\beta} = \hat{\beta}_\infty \frac{R_{\mathrm{eT}}}{12 + R_{\mathrm{eT}}}, \quad \hat{\gamma} = \hat{\gamma}_\infty \frac{12\hat{\gamma}_0 + R_{\mathrm{eT}}}{12 + R_{\mathrm{eT}}} \tag{17}$$

where
$$\hat{\alpha}_\infty = \frac{8 + C_2}{11}, \quad \hat{\beta}_\infty = \frac{8C_2 - 2}{11}, \quad \hat{\gamma}_\infty = \frac{60C_2 - 4}{55} \tag{18}$$

The constants C_1, C_2, and $\hat{\gamma}_0$ 1.8, 0.52, and 0.007, respectively. (19)

Numerical procedure

The equations of the mean and the turbulent fields are discretized using the finite volume method [20] on non-uniform meshes. SIMPLEC algorithm (SIMPLE-Consistent) and power law interpolation scheme (PLDS) are used for pressure-velocity coupling and for the convection-diffusion interpolation term, respectively.

The convergence of the scheme is based on scaled residuals for the continuity, momentum, omega and Reynolds stress components. The scaled residuals for convergence are set between 10^{-6} and 10^{-8}. The solution obtained when all the scaled residuals are less than or equal to this prescribed values and the physical quantities are monotonous. The grids used for all cases presented in this study (wall jet, backward facing step, and cavities) are refined near the walls in order to take into account the viscous sublayer effect.

Boundary conditions

Figure 1 shows the computational domain and the boundary conditions. At inflow boundary [AF], constant velocity profile, turbulent intensity, and turbulent length scale are imposed:

$$U = U_{\mathrm{in}}, \quad V = 0, \quad k = \frac{3}{2}(IU_{\mathrm{in}})^2, \quad \text{and} \quad \omega = \frac{k^{1/2}}{\ell C_\mu^{1/4}}$$

where I is the turbulence intensity rate, ℓ – a turbulent length scale, and C_μ – an empirical constant equal to 0.09 specified in the turbulence model.

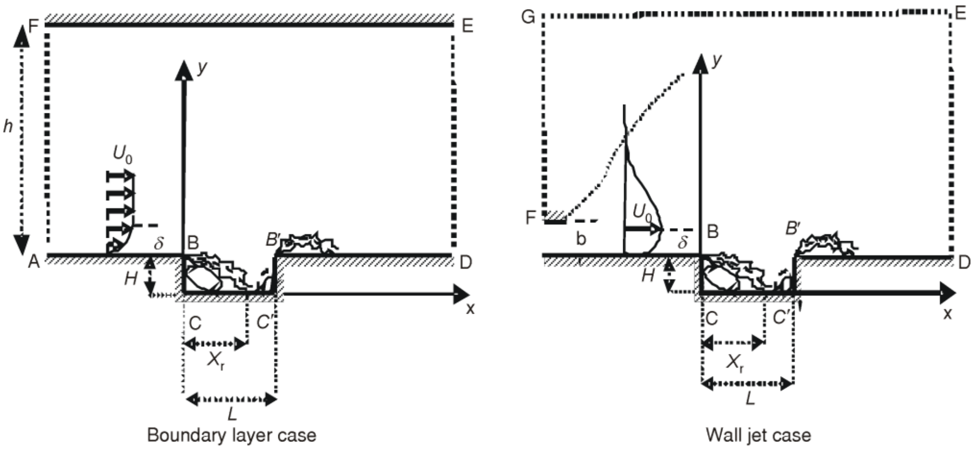

Figure 1. Schematic diagram and computational domain

These values allow having the experimental inlet conditions at the leading edge ($x = 0$). At the outflow boundaries (DE) and (EG), zero pressure is imposed. At the walls, the no-slip boundary conditions ($U = V = 0$) are imposed. Fluent computes the near-wall values of the Reynolds stresses and the specific dissipation rate ω from wall functions.

Results and discussion

Validation

Similarity analysis of wall jet flow

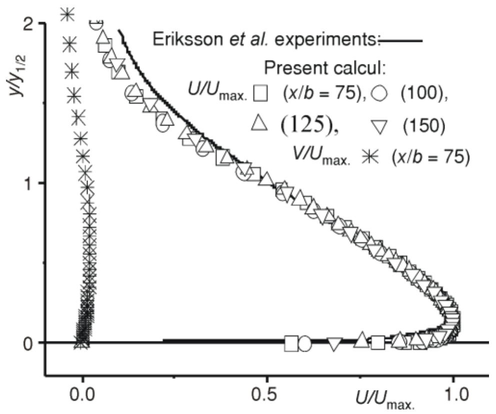

Figure 2. Wall jet mean velocity profile in outer scaling

Initially, a simulation of a wall jet was undertaken in order to verify the similarity of the upstream flow with that of the experimental wall jet. The normalized velocities $U/U_{max.}$ *vs.* $y/y_{1/2}$ have been compared with previous experimental results of Eriksson *et al.* [9] as shown in fig. 2. The good agreement between the numerical prediction with the experimental ones allows us to confirm that the incoming flow is a wall jet flow.

Figure 3 shows a log-log plot of $U_{max.}/U_0$ *vs.* $y_{1/2}/b$. We observe an excellent agreement with the similarity requirement of a power law relation between U_{max} and $y_{1/2}$, *i. e.* $U_{max./}U_0 = B_0(y_{1/2}/b)^n$; the values of $B_0 = 1.084$ and $n = -0.53$ are in perfect accordance with the Karlsson *et al.* experimental ones [21], in which $B_0 = 1.09$ and $n = -0.528$.

Figure 4 displays the dimensionless growth rate of the wall jet, in terms of jet half-width. The half-width $y_{1/2}$, varies linearly with x distance. This numerical result is in a good agreement with the Karlsson *et al*. results [21], Abrahamsson *et al*. results [22], and those of Wygnanski *et al*. experimental ones [23].

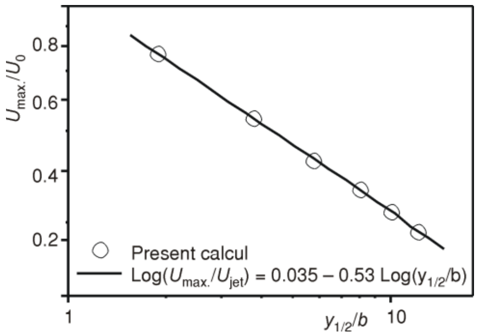

Figure 3. Decay of stream wise mean velocity

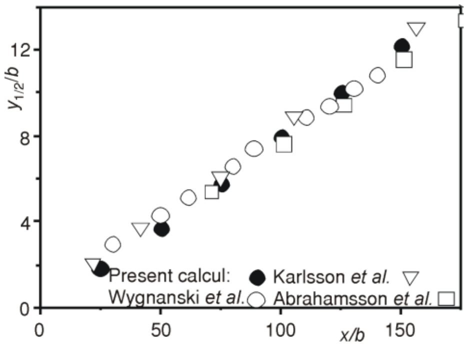

Figure 4. Variation of half-width with downstream distance

Backward facing step under a wall jet flow

Figure 5 shows that, downstream the step, the flow is characterized by the presence of a voluminous recirculation bubble in addition of a smaller corner vortex. The experimental visualisation of Badri [10], confirms this numerical prediction. The experience gives a mean reattachment length of about 3.5 H. The present numerical prediction over-estimates the reattachment length values; it gives $x_r \approx 4.6\ H$. Practically, the same result is obtained by the numerical prediction of Nait Bouda *et al*. [12] where the reattachment length is about 4.5 H.

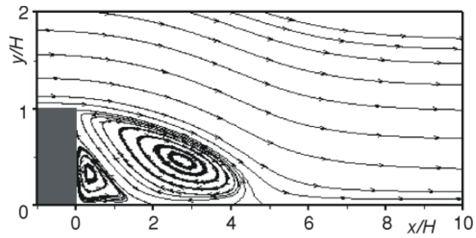

Figure5. Streamlines contours of backward facing step

Figure 6 shows the evolution of the mean longitudinal velocity profiles at six sections within the recirculation, the reattachment and the redevelopment regions. An overall good agreement has been observed with the laser Doppler anemometer (LDA) measurements of Nait Bouda *et al.* [12] and the hot wire (HW) measurements of Badri [10]. The negative values of the velocity confirm the presence of the recirculation zone.

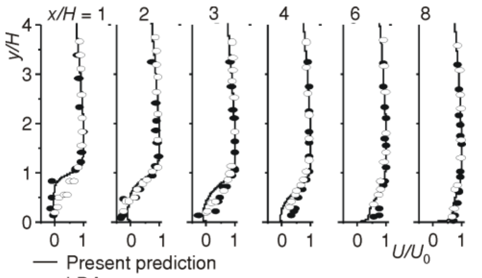

Figure 6. Longitudinal mean velocity profiles at different sections downstream the step

The turbulence intensity profiles, normalized by the local maximum longitudinal velocity U_{max}, are represented in fig. 7. They are compared with the LDA measurements of Nait Bouda *et al*. [12] and with the HW measurements of Badri [10] at the same section of the longitudinal velocity. The results of the present numerical prediction are, on the whole, correct. However, the predicted profiles agree well with the LDA experimental values. A good agreement between the aspect of the numerical profiles and that of the experiments has been observed.

Cavity-flow

The Reynolds number and the boundary layer thickness at the leading edge (x = 0), for the two incoming flows considered in this study are identical and equal to 7600 and 2 cm, respectively.

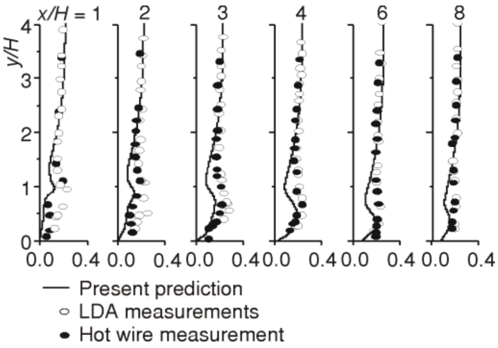

Figure 7. Turbulence intensity $(\overline{u^2})^{1/2}/U_{\max}$ evolution downstream the step

Analysis of the wall static pressure

Figure 8 displays the static pressure distribution at the bottom of the cavities for two different upstream flows: a boundary layer and a wall jet inflow; the pressure coefficients values approach those of Roshko [24]. For the cases considered in this paper, we observe that just behind the upstream step ($x/H \leq 3$) the pressure is uniform then it increases with the increasing x/H.

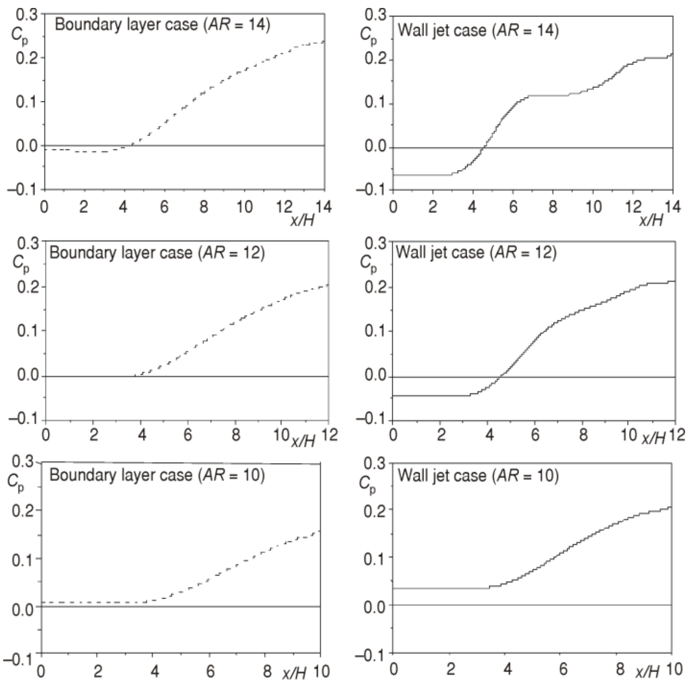

Figure 8. Static pressure coefficients evolution

For AR = 10, under a boundary layer flow, the pressure distribution has a concave-up shape but under a wall jet flow the pressure distribution changes from concave-up shape to a concave-down shape. However, according to the classification of Plentovich *et al*. [25], in the first case the flow is an "open cavity flow" but in the second case it is an "open transitional cavity flow".

For AR = 12, the pressure distribution shows that under a boundary layer, the flow is an "open/ transitional" flow but under a wall jet flow it is a "closed cavity flow", in this latter, an inflection occurs in the pressure distribution.

For AR = 14, under a boundary layer, the flow is a "transitional closed cavity flow" and under a wall jet flow, it is a "closed cavity flow" [25].

Analysis of the mean flow field

Figure 9 illustrates the flow structures of all cases considered in this study. It is interesting to notice the presence of three recirculation bubbles inside the cavity; the principal one is located behind the forward step and two others close to the corners of the cavity. A similar shallow cavity flow structure has been highlighted by the experiments of Avelar *et al.* [26] and by the numerical results of Zdanski *et al.* [27]. In the boundary layer incoming flow, we note that the decrease of the cavity aspect ratio leads a decrease of the distance between the main vortex and the one located in front of the downstream step. These two vortices are touching each other in the cavity of an aspect ratio of 10. These results are in perfect

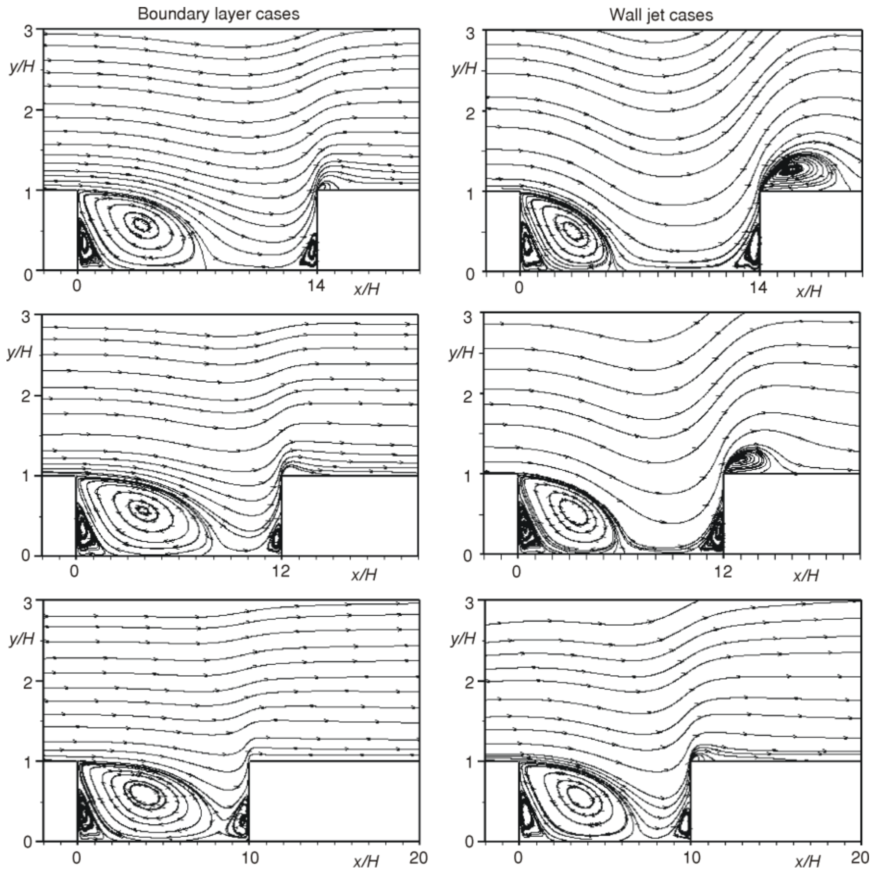

Figure 9. Streamlines contours for the three cavities aspect ratios (*AR* = 14, *AR* = 12, and *AR* = 10)

agreement with the experimental ones of Oka [5] where an analogous flow structure, between two square roughness, was evidenced. It was found that these two vortices are separated by the reattachment boundary layer when the two roughness elements are separated by a distance of 14 *H* while there are touching when this distance is of 9 *H*. In the wall jet incoming flow, the fig. 9 reveals the presence of another recirculation zone over the aft step, which size increase with the increasing of the cavity's aspect ratio.

The skin friction distribution is displayed in fig. 10. The many zero C_f points evidence the presence of more than one vortex. The larger one is formed by the reattachment of the shear layer at the floor, in addition to two corners eddies close to each step. In the

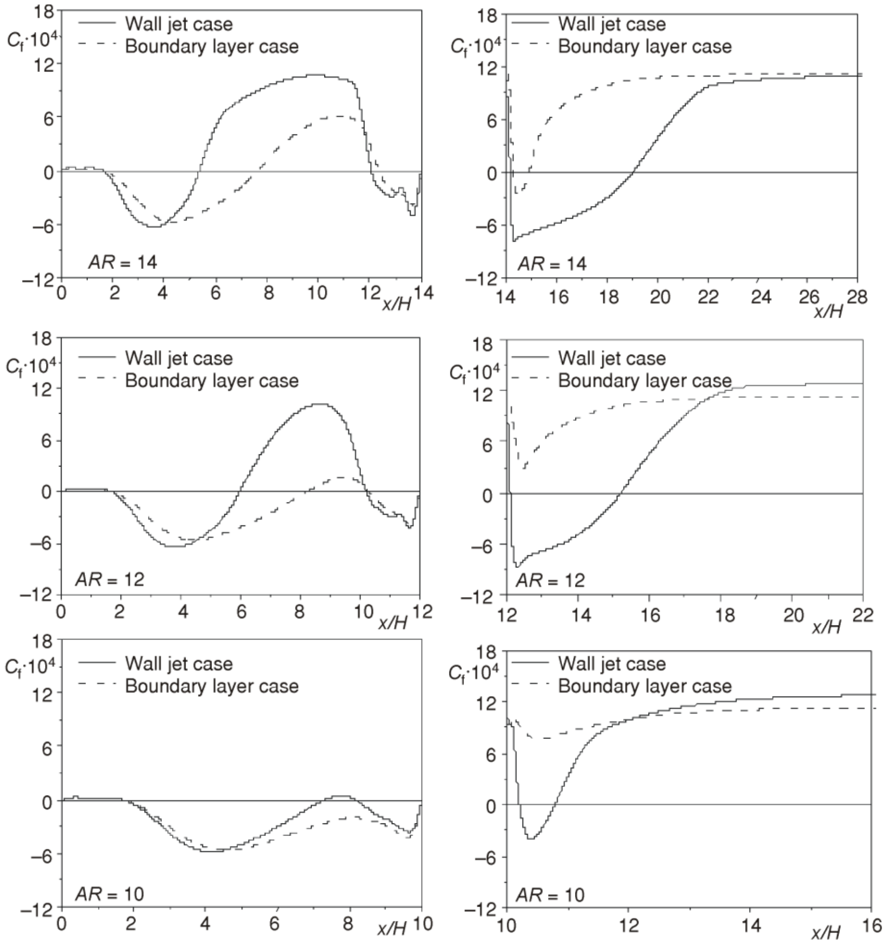

Figure 10. Skin friction coefficients evolution

boundary layer incoming flow, the main vortex length varies between 7 *H* and 8 *H*. This result is in agreement with the experimental ones; it was found that the reattachment point after a single quadratic roughness element in channel flow is at *x/H* = 7 to 8 [4] and the length of the main vortex between two roughness elements is equal to 7 *H* [5]. It is also very interesting to note the reduction of the reattachment length in the wall jet incoming flow; similar phenomenon was observed by several researchers in a wall jet flow over a backward facing step where the reattachment length is much shorter than that measured in duct flow [10-12].

The increase of the maximum of C_f indicates a greater flow-floor friction in the wall jet case.

Analysis of the turbulent flow field

The vorticity contours, plotted in fig. 11, illustrate the presence of two vortical structures: the first one is formed at the leading edge and dragged downstream by the flow, and the second one is produced at the trailing edge and is located above the rearward step. The penetration of the outer layer of the wall jet inside the cavity causes a separation of these two structures, leading to an increase of the second vortices size; particularly for AR = 12 and AR = 14. We notice that the size of this vortex decreases as the cavity's aspect ratio decreases.

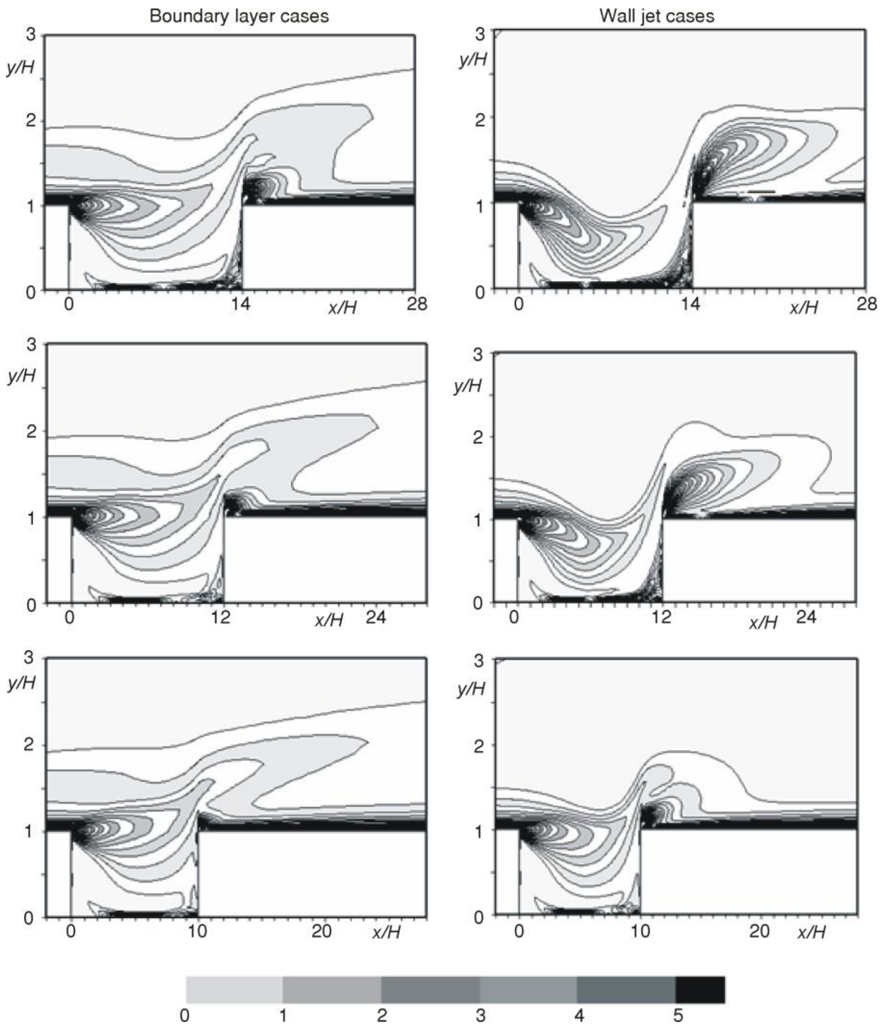

Figure 11. Vorticity contours (30 contours between $\Omega H/U_0$ = 0 and 5)

Figure 12 illustrates the turbulent kinetic energy distribution. The analysis of these figures shows that the cavity gives birth to a shear layer which is the seat of important kinetic energy fluctuations; particularly in the vicinity of the cavity trailing edge where this shear layer impacts. The outer layer, in the wall jet inflow case, is also a source of significant kinetic energy fluctuations. The increases of the cavity's aspect ratio causes a penetration of this external shear layer inside the cavity, thus compressing the internal shear layer.

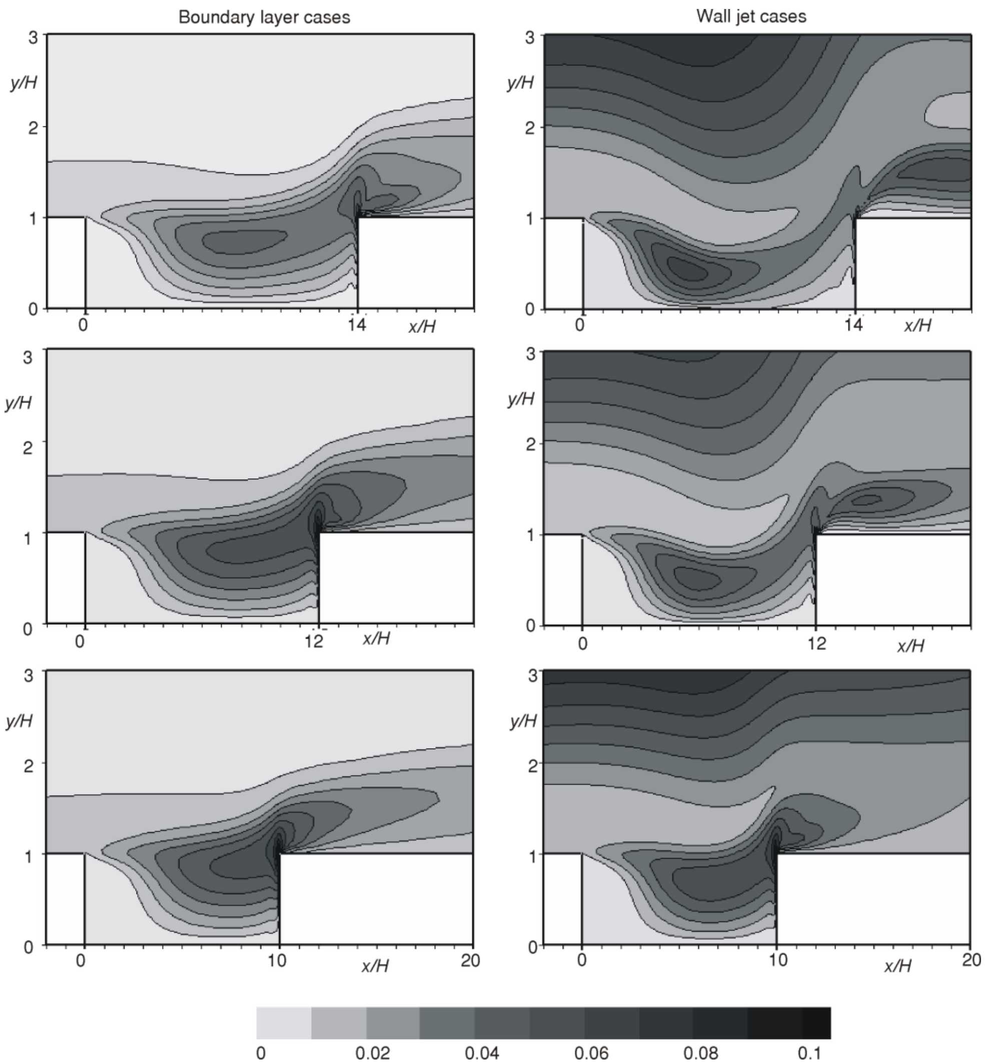

Figure 12. Turbulent kinetic energy contours

Conclusions

The cavity flow is largely used in several practical devices. The major part of previous researches concerns the cavities under a boundary layer flow. The effect of several parameters, on the behaviour of the cavity flow, was the subject of numerous researches since the fifties. Among these parameters: the Mach number, the Reynolds number, the cavity's aspect ratio, and the leading edge boundary layer thickness. The present study deals with the effect of the inflow characteristics on the shallow flow structure and on the reattachment phenomenon. The choice of a cavity under a wall jet flow is dictated by the presence of this configuration in several practical fields in addition to the interest of the wall jets in the industry.

The numerical approach is based on the low-Re stress omega model which is based on the omega equation and LRR model. A numerical prediction of a wall jet flow and a wall jet flow over a backward facing step allowed comparisons with experimental data and the validation of the turbulence model. The results of these preliminary studies are also in good agreement with the previous numerical results based on the RSMKFL2 model.

The numerical prediction of the flow pattern of a shallow cavity reveals the presence of three recirculation zones inside the cavity. The main one is located behind the upstream step and two secondary ones close to the corners of the cavity. In the boundary layer incoming flow, the length of the principal vortex is about 7 H to 8 H in accordance to some previous studies.

However, the reattachment process seems to be accelerated in the wall jet inflow case where the reattachment length is considerably reduced compared to that of the boundary layer inflow case. This reduction can be attributed to an additional turbulent diffusive transfer due to the energetic eddying motions in the external flow layer of the wall jet. This same phenomenon has been observed in the wall jet-backward facing step interaction. Moreover, the penetration of this external layer inside the cavity generates an important bubble above the rearward step, which size's increases with the increasing of the cavity's aspect ratio.

Acknowledgments

The authors wish to thank the polytechnic military School of Algiers (EMP) for their collaboration to use the CFD fluent code.

Nomenclature

AR – cavity aspect ratio (= L/H), [–]
b – nozzle height, [m]
C_f – skin friction coefficient, (= $2\tau_\mathrm{w}/\rho U_0^2$)
C_p – pressure coefficient, (= $2(P - P_\mathrm{ref})/\rho U_0^2$)
H – cavity depth, [m]
k – turbulence kinetic energy, [m^{-2}s^{-2}]
L – cavity length, [m]
P – static pressure, [Nm^{-2}]
Re – Reynolds number (= U_0H/ν), [–]
U – streamwise velocity component, [ms^{-1}]
U_0 – maximum streamwise velocity at $x = 0$, [ms^{-1}]
V – vertical velocity component, [ms^{-1}]
W – cavity width, [m]
x – stream-wise co-ordinate, [m]
x_R – reattachment length, [m]
y – vertical co-ordinate, [m]
$y_{1/2}$ – vertical co-ordinate where $U = U_0/2$, [m]

Greek symbols

δ_{ij} – Kronecker delta, [–]
ν – kinematic viscosity, [m^{2}s^{-1}]
ν_t – turbulent viscosity, [m^{2}s^{-1}]
ρ – fluid density, [kgm^{-3}]
τ_{ij} – Reynolds stress, [m^{2}s^{-2}]
τ_w – wall shear stress, [Nm^{-2}]
ω – specific dissipation rate, [s^{-1}]
Ω_i – mean rate of rotation, [s^{-1}]

References

[1] Mehrez, Z., *et al.*, Mass Transfer Control of a Backward Facing Step Flow by Local Forcing Effect of Reynolds Number, *Thermal Science, 15* (2011), 2, pp. 367-378
[2] Mushatet Khudheyer, S., Simulation of Turbulent Flow and Heat Transfer over a Backward Facing Step with Ribs Turbulators, *Thermal Science, 15* (2011), 1, pp. 245-255
[3] Logan, E., Prapoj, P., Chang, J., A Comparison of Wake Characteristics of Model and Prototype Buildings in Transverse Winds, NASA contractor report No. 3008, 1978

[4] Oka, S., Kostic, Z., Flow Field Past a Single Roughness Element in Channel of Rectangular Cross--Section, in: Heat and Mass Transfer in a Boundary Layer (Eds. N. H. Afgan, Z. Zaric, P. Anastasijevic), Pergamon Press, New York, USA, Vol. 1, pp. 425-435, 1972
[5] Oka, S., Flow Field between Two Roughness Elements in Developed Turbulent Chanel Flow, in: Heat and Mass Transfer in Flows with Separated Regions and Measurement Techniques, Pergamon Press, New York, USA, 1972
[6] Mudgal, B. V., Pani, B. S., Flow Around Obstacles in Plane Turbulent Wall Jets, *Journal of Wind Engineering and Industrial Aerodynamics, 73* (1998), 3, pp. 193-213
[7] Kanna, R. P., Das, M. K., Numerical Simulation of Two-Dimensional Laminar Incompressible offset Jet Flows, *International Journal for Numerical Methods in Fluids*, *49* (2005), 4, pp. 439-464
[8] Bajura, R. A., Szewczyk, A. A., Experimental Investigation of a Laminar Two-Dimensional Plane Wall Jet, *Phys. Fluids, 13* (1970), 7, pp. 1653-1664
[9] Eriksson, J., Karlsson, R. I., Persson, J., An Experimental Study of a Two-Dimensional Plane Turbulent Wall Jet, *J. Experiments in Fluids, 25* (1998), 1, pp. 50-60
[10] Badri, K., Experimental Study of aTurbulent Flow Downstream a Backward Facing Step: a Wall Jet Flow Case and a Boundary Layer Case, Ph. D. thesis (in French), Graduate School for Engineering Sciences, Nantes, France, 1993
[11] Jacob, M. C., *et al*., Experimental Study of Sound Generated by Backward Facing Steps under Wall Jet, *AIAA J*ournal, *392* (2001), 7, pp. 1254-1260
[12] Nait Bouda, N., *et al*., Experimental Approach and Numerical Prediction of Turbulent Wall Jet over a Backward Facing Step, *International Journal of Heat and Fluids Flow, 29* (2008), 4, pp. 927-944
[13] Ganesh, R., Edmane, E., Timoty, J. B, Tone Noise and Nearfield Pressure Produced by Jet-Cavity Interaction, Nasa Technical Report No. TM-20883, 1998
[14] Gloerfelt, X., Bailly, C., Juvé, D., Direct Computational of the Noise Radiation by a Subsonic Cavity Flow and Application of Integral Methods, *Journal of Sound and Vibration*, *266* (2003), pp. 119-146
[15] Ahuja, K. K., Mendoza, J., Effects of Cavity Dimensions, Boundary Layer and Temperature on Cavity Noise with Emphasis on Benchmark Data to Validate Computational Aeroacoustic Codes, NASA Contractor Report No. 4653, 1995
[16] Colonius, T., Basu, A. J., Rowley, C. W., Numerical Investigation of Flow Past a Cavity, AIAA paper, 99 (1912), 5th AIAA/CEAS Aeroacoustics Conference, Greater Seattle, Wa., USA, 1999
[17] Zdanski, P. S. B, *et al*., On the Flow over Cavities of Large Aspect Ratio: A Physical Analysis, *International Communications in Heat and Mass Transfer, 33* (2006), 4, pp. 458-466
[18] Alammar, K. N., Effect of Cavity Aspect Ratio on Flow and Heat Transfer Characteristics in Pipes: A Numerical Study, *Heat and Mass Transfer, 42* (2006), 9, pp. 861-866
[19] Wilcox, D. C., Turbulence Modelling for CFD, 2nd DCW Industries, Inc., La Canada, Cal., USA, 1998
[20] Patankar, S. V., Numerical Heat Transfer and Fluid Flow, *Series in Computational Methods in Mechanics and Thermal Sciences*, Hemisphere Publishing Corporation, New York, USA, 1980
[21] Abrahamsson, H., Johansson, B., Löfdahl, L., A Turbulent Plane Two-Dimensional Wall-Jet in a Quiescent Surrounding, *European Journal of Mechanics. B, Fluids*, *13* (1994), 5, pp. 533-556
[22] Karlsson, R., Eriksson, J., Persson, J., An Experimental Study of a Two-Dimensional Plane Turbulent Wall Jet, Technical report No.VU-S93-B3, Vattenfall Utveckling AB, Älvkarleby Laboratory, Sweden, 1993
[23] Wygnanski, I., Katz, Y., Horev, E., On the Applicability of Various Scaling Laws to the Turbulent Wall jet, *Journal of. Fluid Mechanics, 234* (1992), April, pp. 669-690
[24] Roshko, A., Some Measurements of Flow in a Rectangular Cutout, NACA Technical Note No. 3448, 1955
[25] Plentovich, E. B, Stallings, Jr. R. L., Tracy, M. B., Experimental Cavity Pressure Measurements at Subsonic Speeds, Nasa Technical Paper No. 3358, 1993
[26] Avelar, A. C., Fico, N. G. C. R., Mello, O. A. F., Three-Dimensional Flow over Shallow Cavities, 37th AIAA Fluid Dynamics Conference and Exhibit, Miami, Fla., USA, 4234, 2007
[27] Zdanski, P. S. B, *et al*., Numerical Study of the Flow over Shallow Cavities, *Computers & Fluids*, *32* (2003), 7, pp. 953-974

Paper submitted: December 30, 2010
Paper revised: January 27, 2011
Paper accepted: February, 15, 2011